Mll4 regulates tooth enamel development

Jung-Mi Lee[1,*], Hunmin Jung[1], Qinghuang Tang[1], Woojung An[1], Soo-Kyung Lee[2], Jae W. Lee[2], Yungki Park[3,*], and Hyuk-Jae Edward Kwon[1,*]

[1]Department of Oral Biology, School of Dental Medicine, University at Buffalo, The State University of New York, Buffalo, NY 14214, U.S.A.;
[2]Department of Biological Sciences, College of Arts and Sciences, FOXG1 Research Center, University at Buffalo, The State University of New York, Buffalo, NY 14260, U.S.A.;
[3]Institute for Myelin and Glia Exploration, Department of Biochemistry, Jacobs School of Medicine and Biomedical Sciences, University at Buffalo, The State University of New York, Buffalo, NY 14203, U.S.A.

*Corresponding authors:

Hyuk-Jae Edward Kwon, D.D.S., Ph.D.
Department of Oral Biology, School of Dental Medicine, University at Buffalo, The State University of New York
547 Biomedical Research Building
Buffalo, NY 14214-8024, U.S.A.
Tel: +1-716-829-6301; Fax: +1-716-829-3942; Email: hekwon@buffalo.edu

Jung-Mi Lee, Ph.D.
Department of Oral Biology, School of Dental Medicine, University at Buffalo, The State University of New York
540 Biomedical Research Building
Buffalo, NY 14214-8024, U.S.A.
Tel: +1-716-829-2465; Fax: +1-716-829-3942; Email: jungmile@buffalo.edu

Yungki Park
Institute for Myelin and Glia Exploration, Department of Biochemistry, Jacobs School of Medicine and Biomedical Sciences, University at Buffalo, The State University of New York, Buffalo, NY 14203, U.S.A.
Tel: +1-716-881-7579; Fax: +1-716-849-6651; Email: yungkipa@buffalo.edu

Abstract word count: 299
Word count (Abstract to Acknowledgments): 3,494
Total number of tables/figures: 5 (0 table, 5 figures)
Supplemental appendix: 0 table; 5 figures; Supplemental Materials and Methods
Number of references: 36
6 Keywords: Enamel, Tooth development, Cell differentiation, Gene expression, Epithelia, Morphogenesis

Abstract

Amelogenesis, or enamel development, is a highly regulated process that leads to the formation of tooth enamel, which is critical for protecting teeth from decay and wear. Disruptions in the amelogenesis process can result in amelogenesis imperfecta, a group of genetic conditions characterized by inadequately formed enamel. This condition can include enamel hypoplasia, marked by thinning or underdevelopment of the enamel layer. Mutations in the *MLL4* (*KMT2D*) gene, which encodes a histone H3-lysine 4-methyltransferase, are associated with Kabuki syndrome, a developmental disorder that can involve dental anomalies such as enamel hypoplasia. However, the specific role of MLL4 in amelogenesis and its underlying mechanisms remain poorly understood. To investigate the role of Mll4 in amelogenesis, we generated a conditional knockout mouse line with an ectoderm-specific deletion of *Mll4* (*Krt14-Cre;Mll4*$^{fl/fl}$, or *Mll4*-cKO) and examined the gross, radiographic, histological, cellular, and molecular features in these mice. Micro-computed tomography and scanning electron microscopy analyses revealed that adult *Mll4*-cKO mice exhibited 100% penetrant amelogenesis imperfecta, characterized by hypoplastic and hypomineralized enamel, partially phenocopying human Kabuki syndrome. Additionally, *Mll4*-cKO neonates developed molar tooth germs with minor cusp shape alterations and mild delays in ameloblast differentiation at birth. RNA-seq analysis of the first molar tooth germ at birth revealed that approximately 33.7% of known amelogenesis-related genes were significantly downregulated in the *Mll4*-cKO teeth. Intersection with Mll4 CUT&RUN-seq results identified 8 overlapping genes directly targeted by Mll4. Re-analysis of a single-cell RNA-seq dataset in the developing mouse incisor teeth revealed distinct roles for these genes in Mll4-regulated differentiation across various cell subtypes within the dental epithelium. Among these genes, *Satb1* and *Sp6* are likely directly targeted by Mll4 during the differentiation of pre-ameloblasts into ameloblasts. Taken together, we propose that Mll4 plays a crucial role in amelogenesis by directly activating key genes involved in ameloblast differentiation.

Introduction

Enamel formation, or amelogenesis, is a complex and highly regulated process involving the differentiation and function of ameloblasts. This process is orchestrated by the enamel organ, the epithelial component of the developing tooth germ. The enamel organ initially undergoes morphogenesis through the bud and cap stages, eventually reaching the bell stage, at which it differentiates into four major cell subtypes: the outer enamel epithelium (OEE), stellate reticulum (SR), stratum intermedium (SI), and inner enamel epithelium (IEE). At the end of the bell stage, the IEE cells further differentiate into ameloblasts, marking the onset of amelogenesis. Amelogenesis can be divided into three stages based on ameloblast differentiation and function: presecretory, secretory, and maturation stages, each tightly regulated by a network of genetic and epigenetic factors (Hu et al. 2007; Lacruz et al. 2017). Disruptions in this process can lead to amelogenesis imperfecta, a condition characterized by hypoplastic and/or hypomineralized enamel, which increases the susceptibility to dental caries, injury, hypersensitivity, and aesthetic concerns, ultimately impacting oral health. Therefore, understanding the regulation of amelogenesis is crucial for maintaining dental health and preventing enamel-related defects.

Recent research underscores the crucial role of epigenetic regulation in orofacial organogenesis, particularly the significance of histone modifications in controlling gene expression essential for tooth development (Deng et al. 2020; Kobayashi et al. 2021; Li et al. 2021; Takagiwa et al. 2024; Yu et al. 2022; Zhang et al. 2023; Zhu et al. 2024). Mixed lineage leukemia 4 (MLL4), also known as histone-lysine *N*-methyltransferase 2D (KMT2D), is a key epigenetic regulator that modulates chromatin structure and gene expression by catalyzing the methylation of histone H3 lysine 4 (H3K4) (Froimchuk et al. 2017). MLL4 has been implicated in various organogenesis processes, and mutations in this gene are associated with Kabuki syndrome, a human developmental disorder characterized by distinctive facial features and dental anomalies, including hypodontia, enamel hypoplasia, and delayed tooth eruption (Boniel et al. 2021; Matsune et al. 2001; Porntaveetus et al. 2018). However, the role of MLL4 in tooth development and the mechanisms by which *MLL4* mutations contribute to these dental anomalies, as observed in Kabuki syndrome, remain poorly understood. A recent *in vitro* study using RNA interference-based knockdown in LS8 cells, an immortalized

mouse ameloblast-like cell line derived from the enamel organ of mouse incisors, suggested that Mll4 promotes cell proliferation and maintains self-renewal activity through the activation of Wnt/β-Catenin signaling (Pang et al. 2021). Despite these findings, no *in vivo* studies have definitively established the role of Mll4 in tooth development. This gap in knowledge is likely due, in part, to the early embryonic lethality observed in germline *Mll4* knockout (*Mll4*$^{-/-}$) mice, which die around embryonic day (E) 9.5, well before tooth development begins (Lee et al. 2013).

In this study, we identified a novel role of Mll4 in ameloblast differentiation by rigorously characterizing the tooth developmental process in an ectoderm-specific *Mll4* deletion mouse model, using gross, radiographic, and microscopic observations, as well as molecular assays. Through a combination of RNA-sequencing (RNA-seq) and CUT&RUN-sequencing (CUT&RUN-seq) approaches, we further identified that Mll4 directly targets the transcription of critical genes involved in amelogenesis. Our study provides essential insights into the epigenetic regulation of ameloblast differentiation and enamel formation, highlighting the pivotal role of MLL4 in normal development of enamel and teeth and offering potential therapeutic avenues for amelogenesis-related disorders.

Materials and Methods

Mouse Strains

Krt14-Cre (originally described as '*K14*-Cre') (Andl et al. 2004), and *Mll4*$^{fl/fl}$ (Lee et al. 2013) lines were used for generating an ectoderm-specific *Mll4* conditional knockout (cKO) model. Mice were maintained by intercrossing or by crossing with C57BL/6J inbred mice. All animal procedures were approved by the Institutional Animal Care and Use Committee at the University at Buffalo. This study is compliant with the ARRIVE guidelines (Animal Research Reporting of In Vivo Experiments). Additional detailed information about the experimental procedures is included in the Appendix (Lee et al. 2022).

Results

Mll4 Deficiency in the Dental Epithelium Causes Amelogenesis Imperfecta

To investigate the function of Mll4 in tooth enamel development, we generated a dental epithelium-specific *Mll4*-deficient mouse model (*Mll4*$^{fl/fl}$*;Krt14-Cre*, or *Mll4*-cKO). *Mll4*-cKO mice were born without visible craniofacial anomalies—the palate was successfully fused, and the maxillary and mandibular jaws formed normally (Appendix Fig. 1A). Although they developed scaly skin with scattered hair thinning and exhibited reduced body weights compared to controls, *Mll4*-cKO mice were viable and appeared healthy overall (Appendix Fig. 1B–D) (Egolf et al. 2021). However, upon examining the teeth in adult mice (at 8 weeks), we found that *Mll4*-cKO mice exhibited chalky-white incisors with a rough surface, in contrast to the yellow, smooth-surfaced incisors in control mice (Fig. 1A, E), suggesting a defective enamel layer in the *Mll4*-cKO mice. Micro-computed tomography (CT) analysis of the mandible confirmed that *Mll4*-cKO mice exhibited significantly reduced mineral density and thickness of the enamel in both the incisor and molar teeth (Fig. 1B, C, F, G, Q, Appendix Fig. 2), demonstrating amelogenesis imperfecta in the *Mll4*-cKO tooth enamel. Scanning electron microscopy (SEM) analysis of the molar teeth revealed that *Mll4*-cKO teeth exhibited blunt cusp tips with an irregular enamel surface and poorly formed enamel rods (Fig. 1D, H, R). To determine whether the reduced enamel thickness phenotype, particularly in the cusp tips, was a primary consequence of *Mll4* deficiency or a secondary outcome from post-eruption enamel wear, we further analyzed the tooth enamel phenotype before tooth eruption (at 2 weeks). Consistent with the findings at 8 weeks, *Mll4*-cKO mice at 2 weeks also developed amelogenesis imperfecta with significantly reduced enamel mineral density and thickness as well as a hypoplastic tooth crown. However, the molar teeth did not exhibit the blunt cusp tip phenotype observed at 8 weeks (Fig. 1I–Q). Collectively, these results demonstrate that the *Mll4*-cKO strain exhibits a combination of hypoplastic and hypomineralized amelogenesis imperfecta, indicating that Mll4 is essential for establishing both adequate enamel thickness and mineral density during amelogenesis. Our findings also suggest that the *Mll4*-cKO strain could serve as a novel model for studying amelogenesis and investigating the etiology of dental anomalies associated with Kabuki Syndrome (KS).

Mll4-cKO Teeth Exhibit Minor Cusp Shape Alterations and Mild Delays in Ameloblast Differentiation During Later Embryonic Tooth Development

To identify the developmental mechanisms underlying the role of Mll4 in amelogenesis, we examined the histological features of the first molar in the control and *Mll4*-cKO mice during embryonic tooth development. Hematoxylin and eosin-stained frontal sections of the first molar tooth germ revealed that *Mll4*-cKO embryos exhibited nearly normal tooth morphogenesis throughout the cap (E14.5) and bell (E16.5) stages compared to controls, with minor alterations in cusp shape at E16.5 (Fig. 2A–D). At birth (P0.5), when the transition from the presecretory stage to the secretory stage of amelogenesis begins, *Mll4*-cKO mice showed slightly shorter but broader cusp tips (Fig. 2E, F). Higher magnifications of the cusp tips revealed that *Mll4*-cKO ameloblasts were less polarized and shorter compared to those in controls (Fig. 2G–J), suggesting a critical role for Mll4 in ameloblast differentiation during early amelogenesis. To investigate the cellular mechanisms underlying these developmental phenotypes in the *Mll4*-cKO mice, we analyzed cell proliferation using EdU staining and apoptosis using TUNEL staining at E18.5. We found that *Mll4*-cKO mice exhibited increased cell proliferation in both the pre-ameloblast and pre-odontoblast layers, whereas apoptosis remained unchanged (Appendix Fig. 3A–F). This suggests that an overall developmental delay associated with *Mll4* deficiency may lead to a non-specific increase in cell proliferation in both the dental epithelium and mesenchyme. Additionally, we assessed Mll4 expression through immunofluorescence staining and observed a marked decrease in Mll4 signals in the dental epithelium of the first molar in *Mll4*-cKO mice (Appendix Fig. 4A–D). This finding was further corroborated by real-time qPCR analysis (Appendix Fig. 4E), confirming the successful deletion of epithelial *Mll4* in our mouse model.

Mll4 Regulates Amelogenesis-Related Gene Expression During Early Amelogenesis

To define the molecular mechanisms underlying the gross and microscopic changes observed in the *Mll4*-cKO mouse teeth, we performed genome-wide mRNA expression analysis (RNA-seq) using the first molars from control and *Mll4*-cKO mice at birth (P0.5). Our results revealed 2,366 differentially expressed genes (DEGs), including 1,485 downregulated and 881 upregulated genes, in the *Mll4*-cKO group compared to controls (adjusted *p*-value ≤ 0.001, log2FC ≥ 0.4) (Fig. 3A). Over-representation analysis (ORA) of these DEGs for

enriched gene ontology (GO) terms, as well as gene set enrichment (GSE) analysis, identified that “biomineral tissue development,” “odontogenesis,” “tooth mineralization,” and “amelogenesis” are likely biological processes regulated by Mll4 (Fig. 3B; Appendix Fig. 5). Interestingly, “positive regulation of cell cycle process” was also significantly enriched among the upregulated genes, aligning with the observed increase in cell proliferation in *Mll4*-cKO mice (Appendix Fig. 5). Given the role of Mll4 in modulating transcriptional activation, we focused on further analyzing the downregulated DEGs in the *Mll4*-cKO group. By intersecting the 1,485 downregulated DEGs with 92 amelogenesis-related genes (hereafter “amelogenesis genes”) based on previous findings (Bloch-Zupan et al. 2023; Smith et al. 2017; Wright et al. 2015), we found that approximately 33.7% (31 of 92) of the amelogenesis genes were regulated by Mll4 (Fig. 3C). These genes included those encoding key enamel matrix proteins expressed during ameloblast differentiation, such as amelogenin (*Amelx*), ameloblastin (*Ambn*), and enamelin (*Enam*) (Fig. 3D), which were further validated by real-time qPCR (Fig. 3E). Collectively, these results suggest that Mll4 plays a critical role in early amelogenesis, potentially through the timely activation of gene regulatory programs essential for ameloblast differentiation.

Identification of 8 Candidate Amelogenesis Genes Directly Targeted by Mll4

Next, to identify the direct transcriptional target genes of Mll4, we mapped genome-wide Mll4-binding loci using Mll4 CUT&RUN-seq on wildtype P0.5 mandibular first molars. We identified 2,271 common peaks across two replicates (replicate #1: 4,198 peaks; replicate #2: 3,030 peaks; with 2,271 overlapping peaks), which were used to minimize false-positive results. Approximately 50% of these peaks were located in promoters, while about 47% were found in potential enhancer regions, which includes intronic, intergenic, and immediate downstream regions (Fig. 4A). Using the GREAT tool to identify enriched GO terms, we found that “histone H3 acetylation,” “histone methylation,” and “enamel mineralization” are potential biological processes directly regulated by Mll4. This suggests that Mll4 may play a direct role in amelogenesis, potentially through its function as a histone H3K4 methyltransferase (Fig. 4B). By intersecting the CUT&RUN-seq results with amelogenesis genes, we found that around 14% (13 of 92) of the amelogenesis genes were bound by Mll4 (Fig. 4C). Finally, by integrating the RNA-seq and CUT&RUN-seq results with the amelogenesis genes, we identified 8 overlapping genes directly targeted by Mll4 (Fig. 4C, D).

Mll4 Regulates Distinct Sets of Genes in Different Subtypes of the Enamel Organ During Ameloblast Differentiation

Based on the findings that dental epithelium-specific *Mll4* deletion primarily results in ameloblast differentiation defects (Fig. 2G–J), we compared the mRNA expression patterns of *Mll4* and the 8 candidate genes directly targeted by Mll4, identified through integrating the RNA-seq and CUT&RUN-seq results with amelogenesis genes, across the four major cell subtypes of the dental epithelial enamel organ. We re-analyzed single-cell RNA-seq datasets from the mouse incisor dental epithelium (Chiba et al. 2020) and classified the enamel organ cells into four major subtypes: inner enamel epithelium/outer enamel epithelium (IEE/OEE), stratum intermedium/stellate reticulum (SI/SR), pre-ameloblast (pre-AmB), and ameloblast (AmB) (Fig. 5A). Pseudotemporal trajectories revealed the bifurcation of ameloblast (Fig. 5A, upward arrow) and non-ameloblast lineages (Fig. 5A, downward arrow) from the IEE/OEE, consistent with the current model of amelogenesis (Fresia et al. 2021). *Mll4* was expressed ubiquitously across all enamel organ cell subtypes, though not in every cell (Fig. 5B). By visualizing the co-expression patterns of *Mll4* and the 8 candidate genes, we identified cell type-specific differential gene expression during dental epithelial cell differentiation in the enamel organ. The genes *Cftr, Satb1*, and *Sp6* showed strong overlap in expression patterns with *Mll4*, specifically in pre-AmB and AmB cell subtypes (Fig. 5C, top row), suggesting their potential involvement in Mll4-regulated pre-AmB-to-Amb differentiation. *Gnas* and *Gpr68* exhibited overlapping expression patterns with *Mll4* across pre-AmB, AmB, and SI/SR cell types (Fig. 5C, middle row), indicating their potential roles in both Mll4-regulated AmB and non-AmB differentiation. *Irx5* predominantly co-expressed with *Mll4* in pre-AmB, while *Itgb6* was primarily co-expressed in AmB, and *Gja1* in SI/SR, respectively (Fig. 5C, bottom row). This suggests distinct roles for these genes in Mll4-regulated differentiation within each lineage. Collectively, these findings indicate that Mll4 regulates distinct sets of genes in different dental epithelial cell subtypes of the enamel organ during ameloblast differentiation, underscoring its critical role in the process.

Discussion

In this study, we established that Mll4 is a crucial factor in amelogenesis, as evidenced by the significant reduction in enamel thickness and mineral density observed in the teeth of *Mll4*-cKO mice (Fig. 1), along with defects in ameloblast differentiation (Fig. 2). By integrating CUT&RUN-seq-derived Mll4 target genes (Fig. 4) with RNA-seq-identified downregulated DEGs in *Mll4*-cKO mice (Fig. 3) and previously known amelogenesis-related genes, we identified 8 overlapping genes regulated by Mll4 that are implicated in amelogenesis. Further integration our findings with single-cell transcriptomics datasets revealed the potential distinct roles for these genes in Mll4-regulated differentiation trajectories within the enamel organ (Fig. 5). We finally conducted a literature review, focusing particularly on mouse and human enamel phenotypes associated with these 8 Mll4-regulated amelogenesis genes. Given that *Mll4*-KO mice exhibit defects in ameloblast differentiation at birth, we were primarily interested in the *Cftr*, *Satb1*, and *Sp6* genes, which we identified as being involved in the Mll4-regulated differentiation trajectory from pre-ameloblasts to ameloblasts during early amelogenesis (Fig. 5C, top row). Cftr, primarily known for its role in cystic fibrosis, functions as a chloride ion channel across the cell membrane. In amelogenesis, *Cftr* is expressed in maturation-stage ameloblasts, with structural defects observed only in these maturation-stage ameloblast regions in *Cftr*-deficient mouse incisors (Bronckers et al. 2010). However, enamel defects were restricted to the incisors, with the molars appearing normal in *Cftr*$^{-/-}$ mice (Gawenis et al. 2001). These studies suggest that Cftr may not be the primary factor responsible for the early amelogenesis defects observed in our *Mll4*-cKO model. Nevertheless, it would be intriguing to investigate whether CFTR is involved in Mll4-regulated late-stage amelogenesis, particularly at the maturation stage. Satb1, a transcription factor known for its role as a genome organizer, has been recently been identified as essential for establishing ameloblast cell polarity and regulating enamel formation (Zhang et al. 2019). *Satb1* is highly expressed in presecretory-stage ameloblasts, reduced in secretory-stage ameloblasts, and significantly diminished in maturation-stage ameloblasts. Notably, *Satb1* knockout (*Satb1*$^{-/-}$) mice exhibit a phenotype strikingly similar to our *Mll4*-cKO mice, with defects in ameloblast differentiation during early amelogenesis. Moreover, Kohlschütter-Tönz syndrome-like (KTZSL) disorder, caused by mutations in *SATB1*, shares developmental defects with Kabuki Syndrome, including intellectual disabilities, hypotonia, and enamel

hypoplasia (den Hoed et al. 2021). These findings suggest that Satb1 is a promising candidate through which Mll4 regulates amelogenesis by influencing the differentiation of pre-ameloblasts into ameloblasts. Sp6, known to induce hypoplastic amelogenesis imperfecta in humans, is expressed in both presecretory- and secretory-stage ameloblasts and regulates both cell proliferation and differentiation in ameloblasts (Bloch-Zupan et al. 2023; Nakamura et al. 2004). Mice deficient in *Sp6* (*Epfn*$^{-/-}$) show enamel deficiencies, as well as defects in cusp and root formation and abnormal dentin structure (Nakamura et al. 2008). Recent research has identified Sp6 as a master regulator that directly controls the expression of *Amelx*, *Ambn*, and *Enam* during tooth development (Rhodes et al. 2021). These studies indicate that Sp6 may also be a key mediator in Mll4-regulated early-stage amelogenesis, making it a promising candidate for further investigation in this context.

Among the other candidate genes, *Gpr68*, *Itgb6*, and *Gja1* have been studied in mouse models. Deficiencies in *Gpr68* (*Ogr1*$^{-/-}$) do not result in significant enamel defects, whereas deficiencies in either *Itgb6* (*Itgb6*$^{-/-}$) or *Gja1* (*Gja1*$^{Jrt/+}$) lead to enamel hypoplasia (Flenniken et al. 2005; Mohazab et al. 2013; Parry et al. 2016; Wazen et al. 2015). Itgb6 is a cell surface adhesion receptor that mediates cell-cell and cell-extracellular matrix interactions and is expressed in maturation-stage ameloblasts; *Itgb6*$^{-/-}$ mice also exhibit a hypomineralized amelogenesis imperfecta phenotype (Smith et al. 2017). Gja1, a gap junction protein, is expressed in both secretory- and maturation-stage ameloblasts, and mice with heterozygous *Gja1* mutation (*Gja1*$^{Jrt/+}$) show hypoplastic enamel defects (Toth et al. 2010). Given the established phenotypes in these mice, we speculate that *Itgb6* and *Gja1* may mediate Mll4-regulated amelogenesis, specifically associated with the maturation-stage ameloblasts.

Our major findings align with previous research on histone-modifying epigenetic factors in tooth development (Deng et al. 2020; Kobayashi et al. 2021; Li et al. 2021; Takagiwa et al. 2024; Yu et al. 2022; Zhang et al. 2023; Zhu et al. 2024). However, our study is the first to specifically implicate Mll4 in the regulation of amelogenesis in an *in vivo* model. It has been reported that *KMT2D* deficiency disturbs the cell cycle activity in the LS8 dental epithelial cell line (Pang et al. 2021), which contrasts with our findings of increased proliferation in the *Mll4*-cKO tooth germ compared to controls. We speculate that this discrepancy arises from differences between the cell line and mouse model systems, as an *in vitro* cell line model may not fully recapitulate the complex microenvironment and signaling interactions present *in vivo*.

This study not only advances our understanding of the molecular mechanisms underlying amelogenesis but also suggests potential epigenetic therapeutic targets for treating amelogenesis imperfecta. While our research provides significant molecular insights into Mll4-regulated gene programs that control ameloblast differentiation during early-stage amelogenesis, it would be valuable to explore whether these regulatory mechanisms also play a role in late-stage amelogenesis. The recent development of new Cre driver lines through the NIH NIDCR FaceBase initiative, including *Ambn-Cre*, *Amelx-Cre,* and *Odam-Cre* (Samuels et al. 2020), presents a valuable opportunity to investigate Mll4's role at different stages of enamel formation. Future studies utilizing these stage-specific Cre-driver models can help delineate Mll4's function across different stages of amelogenesis. Additionally, examining potential interactions between Mll4 and other histone modifiers in enamel formation and investigating similar mechanisms in other mineralized tissues would be beneficial.

Author Contributions

J.-M. Lee, H.-J.E. Kwon, contributed to conception, design, data acquisition and interpretation, performed statistical analyses, drafted, and critically revised the manuscript. H. Jung, Q. Tang, W. An, contributed to data acquisition and interpretation, performed statistical analyses, and critically revised the manuscript. S.-K. Lee, J.W. Lee, contributed to conception, design, and critically revised the manuscript. Y. Park, contributed to data interpretation, performed statistical analyses, and critically revised the manuscript. All authors gave final approval and agree to be accountable for all aspects of the work.

Acknowledgements

We acknowledge the assistance of Liwen Li, PhD (University at Buffalo); Victor Yuan (University at Buffalo); Andrew McCall, PhD (University at Buffalo); and Peter Bush (University at Buffalo), in various aspects of the current study. Micro-CT and light microscopy data in this study were acquired at the Optical Imaging and Analysis Facility, School of Dental Medicine, State University of New York at Buffalo. SEM data were acquired at the South Campus Instrument Center, School of Dental Medicine, State University of New York at Buffalo. Finally, we thank the members of the Kwon lab and our colleagues in the Department of Oral Biology for their helpful comments and feedback.

Funding

This study was supported by the National Institutes of Health's (NIH's) National Center for Advancing Translational Sciences (KL2TR001413 and UL1TR001412 to H-JEK), National Institute of Dental and Craniofacial Research (T32DE023526 to J-ML; R03DE030985 to H-JEK), and National Institute of Neurological Disorders and Stroke (1R21NS123775-01 to YP; R01NS118748 to JWL and S-KL; R01NS100471 and R01NS111760 to S-KL).

Declaration of Conflicting Interests

The authors declared no potential conflicts of interest with respect to the research, authorship, and/or publication of this article.

References

Andl T, Ahn K, Kairo A, Chu EY, Wine-Lee L, Reddy ST, Croft NJ, Cebra-Thomas JA, Metzger D, Chambon P et al. 2004. Epithelial bmpr1a regulates differentiation and proliferation in postnatal hair follicles and is essential for tooth development. Development. 131(10):2257-2268.

Bloch-Zupan A, Rey T, Jimenez-Armijo A, Kawczynski M, Kharouf N, de La Dure-molla M, Noirrit E, Hernandez M, Joseph-Beaudin C, Lopez S et al. 2023. : Next-generation sequencing sheds light on witkop's classification. Frontiers in Physiology. 14.

Boniel S, Szymańska K, Śmigiel R, Szczałuba K. 2021. Kabuki syndrome-clinical review with molecular aspects. Genes (Basel). 12(4).

Bronckers A, Kalogeraki L, Jorna HJN, Wilke M, Bervoets TJ, Lyaruu DM, Zandieh-Doulabi B, DenBesten P, de Jonge H. 2010. The cystic fibrosis transmembrane conductance regulator (cftr) is expressed in maturation stage ameloblasts, odontoblasts and bone cells. Bone. 46(4):1188-1196.

Chiba Y, Saito K, Martin D, Boger ET, Rhodes C, Yoshizaki K, Nakamura T, Yamada A, Morell RJ, Yamada Y et al. 2020. Single-cell rna-sequencing from mouse incisor reveals dental epithelial cell-type specific genes. Front Cell Dev Biol. 8:841.

den Hoed J, de Boer E, Voisin N, Dingemans AJM, Guex N, Wiel L, Nellaker C, Amudhavalli SM, Banka S, Bena FS et al. 2021. Mutation-specific pathophysiological mechanisms define different neurodevelopmental disorders associated with satb1 dysfunction. Am J Hum Genet. 108(2):346-356.

Deng H, Fujiwara N, Cui H, Whitford GM, Bartlett JD, Suzuki M. 2020. Histone acetyltransferase promotes fluoride toxicity in ls8 cells. Chemosphere. 247:125825.

Egolf S, Zou J, Anderson A, Simpson CL, Aubert Y, Prouty S, Ge K, Seykora JT, Capell BC. 2021. Mll4 mediates differentiation and tumor suppression through ferroptosis. Sci Adv. 7(50).

Flenniken AM, Osborne LR, Anderson N, Ciliberti N, Fleming C, Gittens JE, Gong XQ, Kelsey LB, Lounsbury C, Moreno L et al. 2005. A gja1 missense mutation in a mouse model of oculodentodigital dysplasia. Development. 132(19):4375-4386.

Fresia R, Marangoni P, Burstyn-Cohen T, Sharir A. 2021. From bite to byte: Dental structures resolved at a single-cell resolution. Journal of Dental Research. 100(9):897-905.

Froimchuk E, Jang Y, Ge K. 2017. Histone h3 lysine 4 methyltransferase kmt2d. Gene. 627:337-342.

Gawenis LR, Spencer P, Hillman LS, Harline MC, Morris JS, Clarke LL. 2001. Mineral content of calcified tissues in cystic fibrosis mice. Biol Trace Elem Res. 83(1):69-81.

Hu JC, Chun YH, Al Hazzazzi T, Simmer JP. 2007. Enamel formation and amelogenesis imperfecta. Cells Tissues Organs. 186(1):78-85.

Kobayashi Y, Quispe-Salcedo A, Bodas S, Matsumura S, Li EH, Johnson R, Choudhury M, Fine DH, Nadimpalli S, Duncan HF et al. 2021. Knockout in mesenchymal cells causes enamel hyper-mineralization. Biochem Bioph Res Co. 567:72-78.

Lacruz RS, Habelitz S, Wright JT, Paine ML. 2017. Dental enamel formation and implications for oral health and disease. Physiol Rev. 97(3):939-993.

Lee JE, Wang C, Xu S, Cho YW, Wang L, Feng X, Baldridge A, Sartorelli V, Zhuang L, Peng W et al. 2013. H3k4 mono- and di-methyltransferase mll4 is required for enhancer activation during cell differentiation. Elife. 2:e01503.

Lee JM, Qin C, Chai OH, Lan Y, Jiang R, Kwon HE. 2022. Msx1 drives tooth morphogenesis through controlling wnt signaling activity. J Dent Res. 101(7):832-839.

Li H, Cui D, Zheng L, Zhou Y, Gan L, Liu Y, Pan Y, Zhou X, Wan M. 2021. Bisphenol a exposure disrupts enamel formation via ezh2-mediated h3k27me3. Journal of Dental Research. 100(8):847-857.

Matsune K, Shimizu T, Tohma T, Asada Y, Ohashi H, Maeda T. 2001. Craniofacial and dental characteristics of kabuki syndrome. Am J Med Genet. 98(2):185-190.

Mohazab L, Koivisto L, Jiang GQ, Kytömäki L, Haapasalo M, Owen GR, Wiebe C, Xie YS, Heikinheimo K, Yoshida T et al. 2013. Critical role for αvβ6 integrin in enamel biomineralization. J Cell Sci. 126(3):732-744.

Nakamura T, de Vega S, Fukumoto S, Jimenez L, Unda F, Yamada Y. 2008. Transcription factor epiprofin is essential for tooth morphogenesis by regulating epithelial cell fate and tooth number. J Biol Chem. 283(8):4825-4833.

Nakamura T, Unda F, de-Vega S, Vilaxa A, Fukumoto S, Yamada KM, Yamada Y. 2004. The krüppel-like factor epiprofin is expressed by epithelium of developing teeth, hair follicles, and limb buds and promotes cell proliferation. J Biol Chem. 279(1):626-634.

Pang LP, Tian H, Gao XJ, Wang WP, Wang XY, Zhang ZC. 2021. Kmt2d deficiency disturbs the proliferation and cell cycle activity of dental epithelial cell line (ls8) partially via wnt signaling. Bioscience Rep. 41(11).

Parry DA, Smith CE, El-Sayed W, Poulter JA, Shore RC, Logan CV, Mogi C, Sato K, Okajima F, Harada A et al. 2016. Mutations in the ph-sensing g-protein-coupled receptor gpr68 cause amelogenesis imperfecta. Am J Hum Genet. 99(4):984-990.

Porntaveetus T, Abid MF, Theerapanon T, Srichomthong C, Ohazama A, Kawasaki K, Kawasaki M, Suphapeetiporn K, Sharpe PT, Shotelersuk V. 2018. Expanding the oro-dental and mutational spectra of kabuki syndrome and expression of kmt2d and kdm6a in human tooth germs. Int J Biol Sci. 14(4):381-389.

Rhodes CS, Yoshitomi Y, Burbelo PD, Freese NH, Nakamura T, Chiba Y, Yamada Y, Computational NNG. 2021. Sp6/epiprofin is a master regulator in the developing tooth. Biochem Bioph Res Co. 581:89-95.

Samuels BD, Aho R, Brinkley JF, Bugacov A, Feingold E, Fisher S, Gonzalez-Reiche AS, Hacia JG, Hallgrimsson B, Hansen K et al. 2020. Facebase 3: Analytical tools and fair resources for craniofacial and dental research. Development. 147(18).

Smith CEL, Poulter JA, Antanaviciute A, Kirkham J, Brookes SJ, Inglehearn CF, Mighell AJ. 2017. Amelogenesis imperfecta; genes, proteins, and pathways. Front Physiol. 8:435.

Takagiwa Y, Higashihori N, Kano S, Moriyama K. 2024. Roles of the histone methyltransferase set domain bifurcated 1 in epithelial cells during tooth development. Arch Oral Biol. 165:106026.

Toth K, Shao Q, Lorentz R, Laird DW. 2010. Decreased levels of cx43 gap junctions result in ameloblast dysregulation and enamel hypoplasia in gja1jrt/+ mice. J Cell Physiol. 223(3):601-609.

Wazen RM, Moffatt P, Ponce KJ, Kuroda S, Nishio C, Nanci A. 2015. Inactivation of the odontogenic ameloblast-associated gene affects the integrity of the junctional epithelium and gingival healing. Eur Cells Mater. 30:187-199.

Wright JT, Carrion IA, Morris C. 2015. The molecular basis of hereditary enamel defects in humans. J Dent Res. 94(1):52-61.

Yu F, Li F, Zheng L, Ye L. 2022. Epigenetic controls of sonic hedgehog guarantee fidelity of epithelial adult stem cells trajectory in regeneration. Sci Adv. 8(29):eabn4977.

Zhang Y, Li HY, Cui DX, Liu Y, Tian QL, Zheng LW, Wan M. 2023. Epigenetics in developmental defects of enamel: A scoping review. Oral Dis. 29(6):2366-2375.

Zhang Y, Zheng LW, Le M, Nakano Y, Chan B, Huang YL, Torbaty PM, Kohwi Y, Marcucio R, Habelitz S et al. 2019. Satb1 establishes ameloblast cell polarity and regulates directional amelogenin secretion for enamel formation. Bmc Biol. 17(1).

Zhu X, Ma Z, Xie F, Wang J. 2024. Ash2l, core subunit of h3k4 methylation complex, regulates amelogenesis. Journal of Dental Research. 103(1):81-90.

Figure Legends

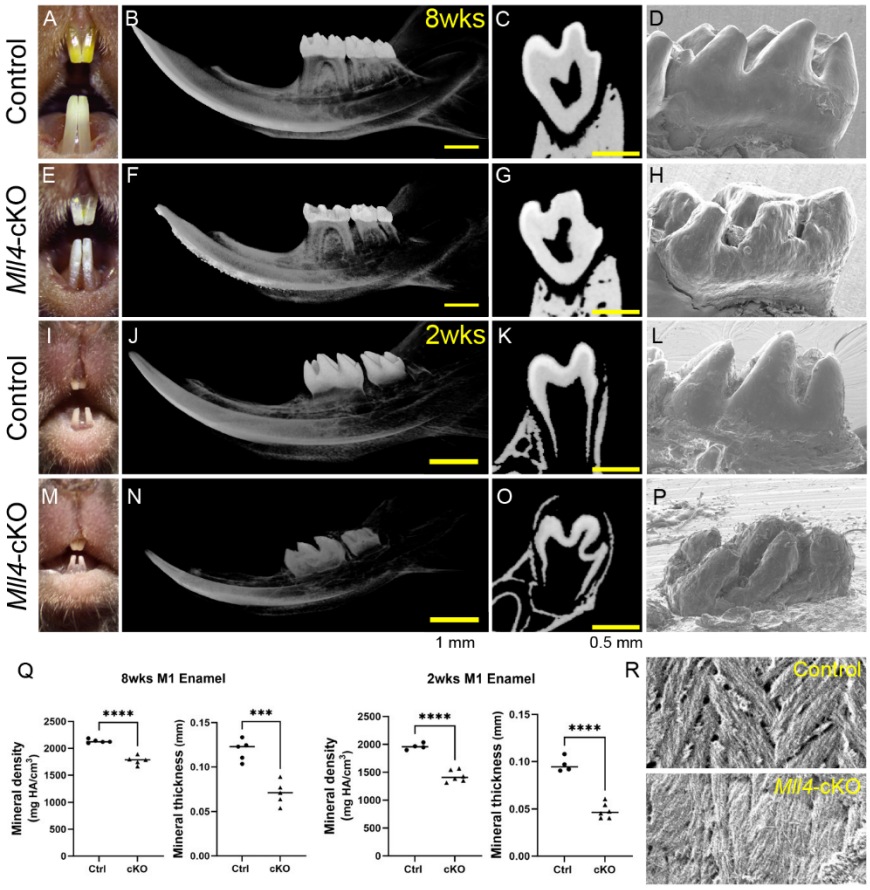

Figure 1. *Mll4*-cKO mice exhibit defective enamel, phenocopying human Kabuki syndrome. (A–D, E–H, I–L, M–P) Comparison of control and dental epithelium-specific conditional *Mll4*-deficiency (*Mll4*-cKO) mouse teeth at 8 weeks (A–H) and 2 weeks (I–P). *Mll4*-cKO mice exhibited chalky-white incisors with a rough surface (E) compared to control incisors, which were yellow and had a smooth surface (A), at 8 weeks. Micro-CT analysis of the mandible showed a defective enamel layer with reduced radiopacity and thickness in the *Mll4*-cKO incisor and molar teeth at both 8 and 2 weeks (F, G, N, O), compared to controls (B, C, J, K). Panels C, G, K, and O are frontal/coronal slices of the first molar in B, F, J, and N. (D, H, L, P) SEM images of the first molar tooth crown from control (D, L) and *Mll4*-cKO mice (H, P) showed that *Mll4*-cKO teeth exhibit blunt cusp tips at 8 weeks (D, H) and a hypoplastic crown at 2 weeks (L, P). (Q) Quantification of enamel mineral density and thickness in the first molars from control and *Mll4*-cKO mice at 8 weeks and 2 weeks. (R) SEM images of enamel rod microstructures in control and *Mll4*-cKO mice. Scale bars: 1 mm (in B, F, J, N) and 0.5 mm (in C, G, K, O). M1, first molar. ***$p < 0.001$; ****$p < 0.0001$. $n = 4–6$ per group.

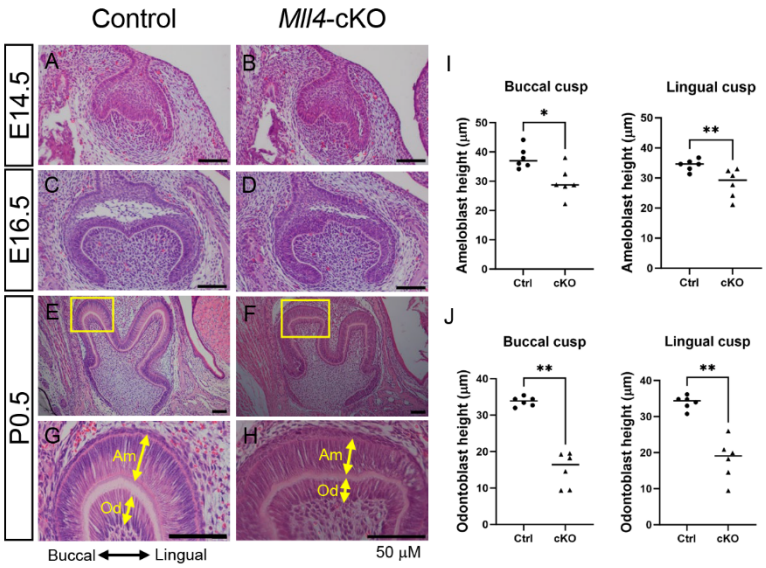

Figure 2. *Mll4*-cKO mouse embryos exhibit nearly normal tooth morphogenesis, with minor alterations in cusp shape and ameloblast cell polarization at birth. (A–F) Hematoxylin and eosin staining of frontal sections of the first molar tooth germ in control (A, C, E) and *Mll4*-cKO mice (B, D, F) at E14.5 (A, B), E16.5 (C, D), and P0.5 (E, F). (G, H) Higher magnifications of the buccal cusp (yellow boxes in panels E and F) show broadened cusp tips with shorter ameloblasts and odontoblasts in the *Mll4*-cKO mice compared to controls. Scale bars: 50 μm (in panels A–H). Am, ameloblast; Od, odontoblast. The black double-headed arrow indicates buccal and lingual directions. (I, J) Quantification of ameloblast (I) and odontoblast (J) heights in the buccal and lingual cusps, as shown in panels G and H. *$p < 0.05$; **$p < 0.01$. $n = 6$ per group.

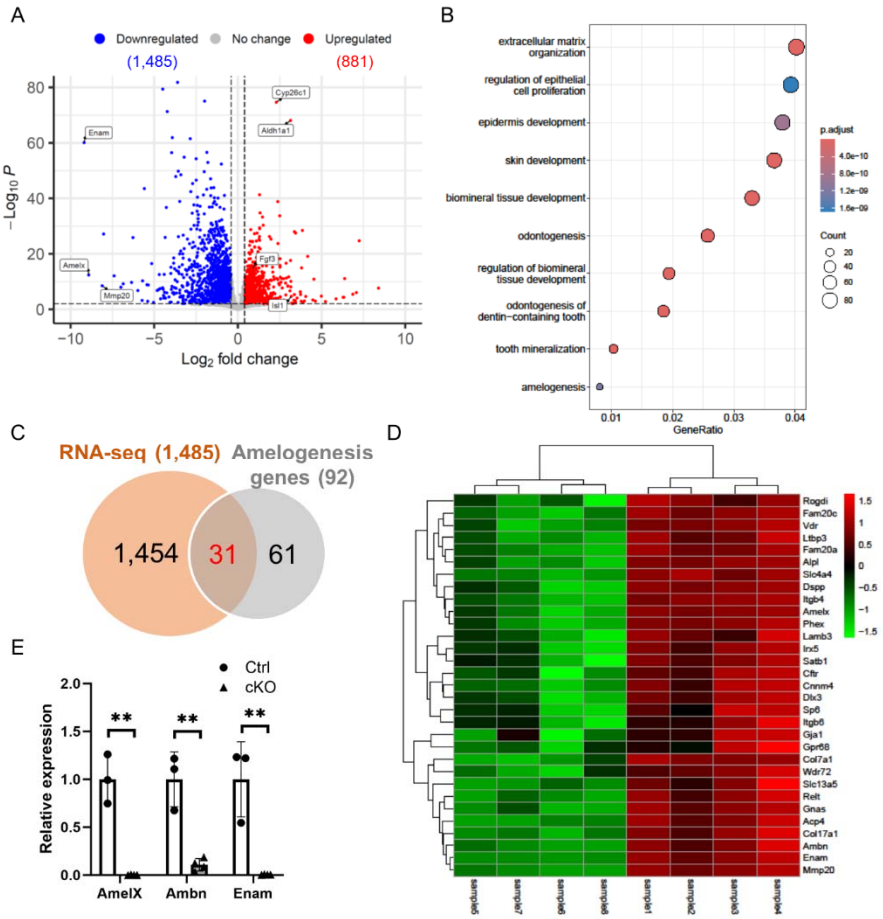

Figure 3. Mll4 regulates amelogenesis-related gene expression in the molar tooth germ. (A–D) Genome-wide mRNA expression analysis in control and *Mll4*-cKO first molars at P0.5. (A) Volcano plot showing a total of 2,366 differentially expressed genes (DEGs)—881 upregulated and 1,485 downregulated (adjusted *p*-value ≤ 0.001, log2FC ≥ 0.4). (B) Enriched gene ontology (GO) biological processes from over-representation analysis (ORA) of the significant DEGs. (C) Intersection of the downregulated DEGs and 92 genes related to amelogenesis, showing that approximately 33.7% (31 of 92) of amelogenesis genes overlap with the downregulated DEGs. (D) Heatmap of the 31 overlapping genes identified in panel C. (E) Real-time qPCR results for key amelogenesis genes (*Amelx, Ambn,* and *Enam*) selected from these 40 overlapping genes, validating the significantly decreased expression in the *Mll4*-cKO first molar compared to control. ***p* < 0.01. *n* = 3–4 per group.

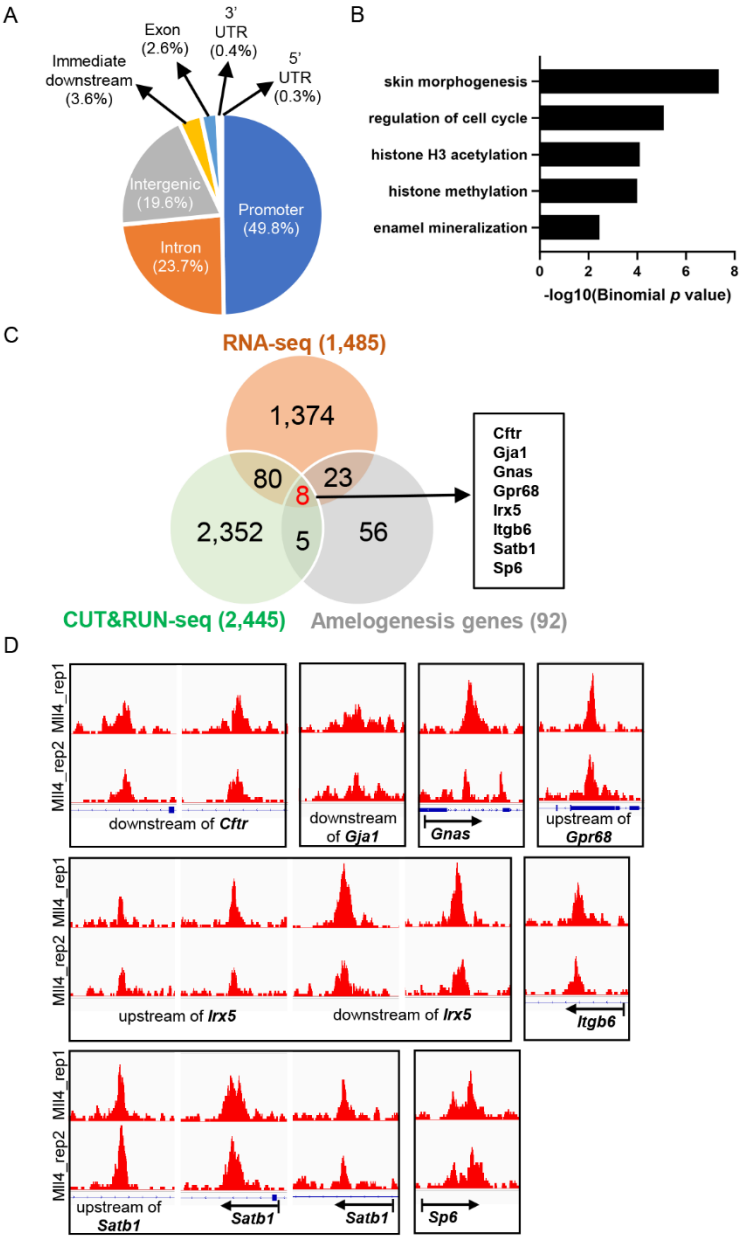

Figure 4. Identification of amelogenesis-related genes directly targeted by Mll4. (A–D) Mll4 CUT&RUN-seq analysis results in wildtype first molars at P0.5, with two replicates. (A) Distribution pattern of the Mll4 binding peaks across genomic regions. (B) Enriched GO biological processes associated with Mll4 binding peaks using the GREAT tool. (C) Three-way intersection of CUT&RUN-seq-based Mll4 target genes, RNA-seq-based *Mll4*-cKO downregulated DEGs (as identified in Figure 3C), and 92 amelogenesis genes, identifying 8 overlapping genes directly targeted by Mll4. (D) Mll4 binding loci near the identified 8 direct target genes of Mll4 from two CUT&RUN-seq replicates (Mll4_rep1 and Mll4_rep2).

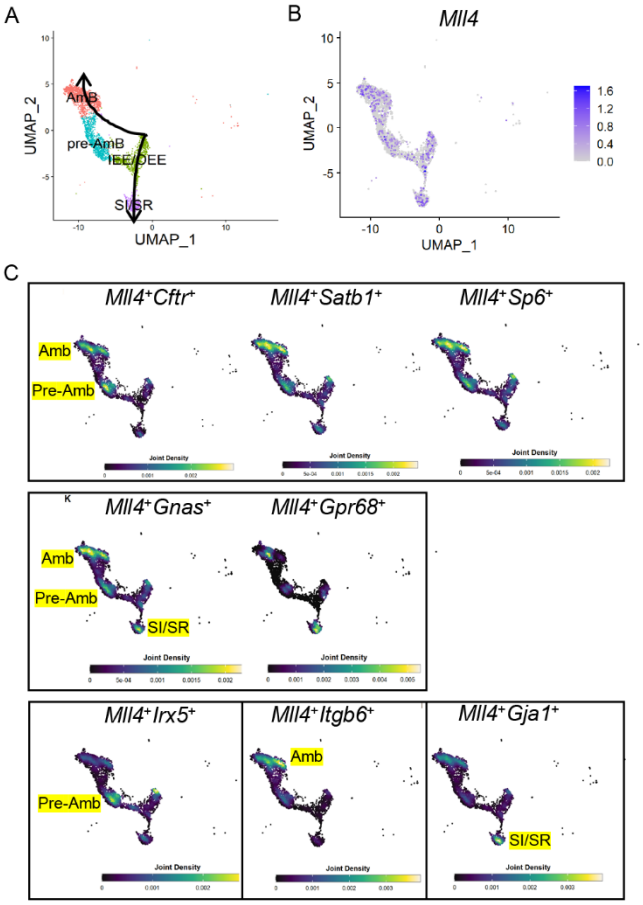

Figure 5. Cell subtype-specific differential gene expression analysis reveals a distinct involvement of Mll4 target genes during the differentiation of dental epithelium.
(A–C) Re-analysis of a single-cell RNA-seq dataset from P7 mouse incisors. (A) Uniform Manifold Approximation and Projection (UMAP) showing the classification of the dental epithelial cells into four major cell types: inner enamel epithelium/outer enamel epithelium (IEE/OEE), stratum intermedium/stellate reticulum (SI/SR), pre-ameloblast (pre-AmB), and ameloblast (AmB). The UMAP also indicates the pseudotemporal trajectories of these cell types, with arrows showing the bifurcation of ameloblast and non-ameloblast cells (arrows). (B) Identification of cell subtypes expressing *Mll4*. (C) Joint density plots visualizing the co-expression patterns of 8 target genes with *Mll4*.

Supplemental Figures

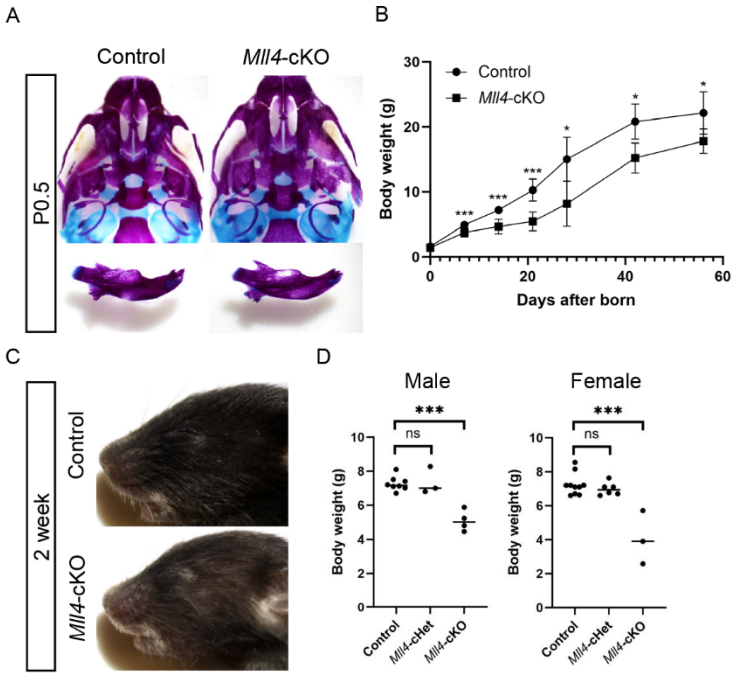

Appendix Figure 1. *Mll4*-cKO mice did not show visible craniofacial anomalies but exhibited hair thinning and reduced body weight. (A) Skeletal staining of the maxillary (top row) and mandibular jaws (bottom row). Overall skeletal structures were similar between control and *Mll4*-cKO mice at birth (P0.5). (B) Body weight kinetics showing significantly reduced body weight in the *Mll4*-cKO mice compared to controls at all postnatal time points. (C) Lateral view of the craniofacial region at 2 weeks, showing scattered hair thinning but no visible craniofacial differences between control and *Mll4*-cKO mice. (D) Body weights of control, *Mll4*-cHet, and *Mll4*-cKO mice, both male and female, at 2 weeks. No significant difference was found between control and *Mll4*-cHet mice. However, *Mll4*-cKO mice showed significantly reduced body weight compared to controls. *$p < 0.05$; ***$p < 0.001$; ns, $p > 0.05$. n = 3–10 per group.

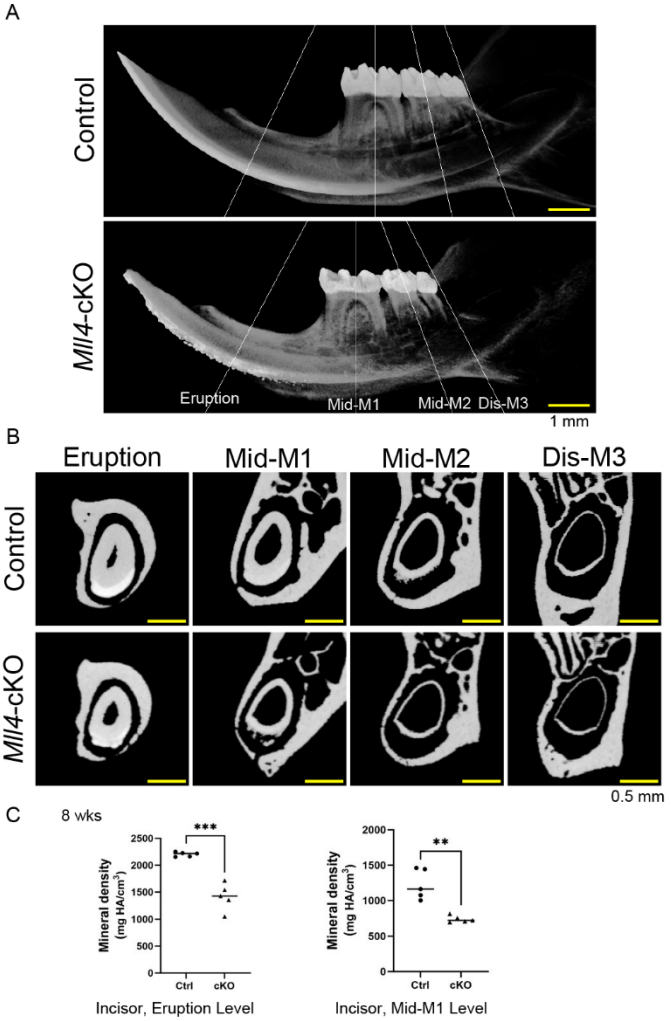

Appendix Figure 2. Defective enamel in the *Mll4*-cKO mouse incisor. (A, B) Micro-CT-based comparison of control and *Mll4*-cKO mouse incisors at 8 weeks. (A) 3D volume-rendered images, or pseudo-x-ray views, showing four representative section planes along the anteroposterior axis of the mandible, based on skeletal and dental anatomical landmarks. (B) Transverse section images at the four representative planes, corresponding to the levels of eruption of the incisor, the midsection of M1, the midsection of M2, and the distal section of M3. (C) Quantification of enamel mineral density in the incisors at the eruption level and the midsection of M1 for both control and *Mll4*-cKO mice at 8 weeks. M1, M2, and M3 refer to the first, second, and third molar. Scale bars: 1 mm (in panel A) and 0.5 mm (in panel B). $^{**}p < 0.01$; $^{***}p < 0.001$. $n = 5–6$ per group.

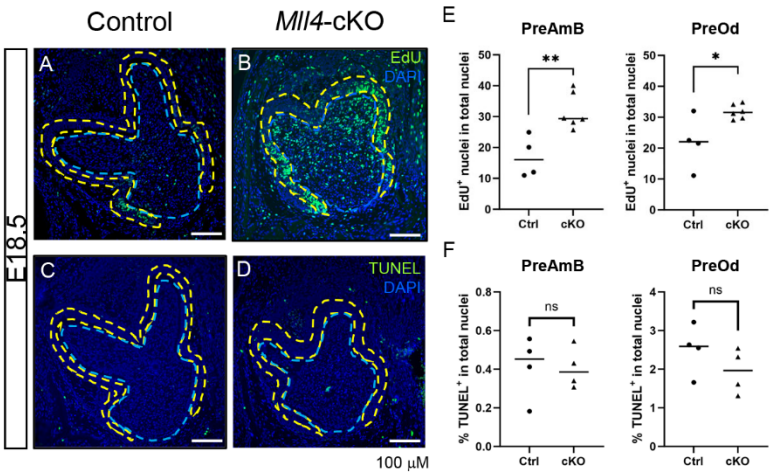

Appendix Figure 3. *Mll4*-cKO mouse embryos exhibited increased proliferation in both the pre-ameloblast and pre-odontoblast layers, while apoptosis remained unchanged. (A, B, E) EdU staining showed increased proliferation pre-ameloblast (dental epithelial) and pre-odontoblast (dental mesenchymal) layers of the *Mll4*-cKO first molars compared to controls at E18.5. (C, D, F) TUNEL staining revealed no significant changes in apoptosis in either layer. PreAmB, pre-ameloblast (outlined with yellow dashed lines); PreOd, pre-odontoblast (outlined with light blue dashed lines). *$p < 0.05$; **$p < 0.01$; ns, $p > 0.05$. $n = 4–6$ per group.

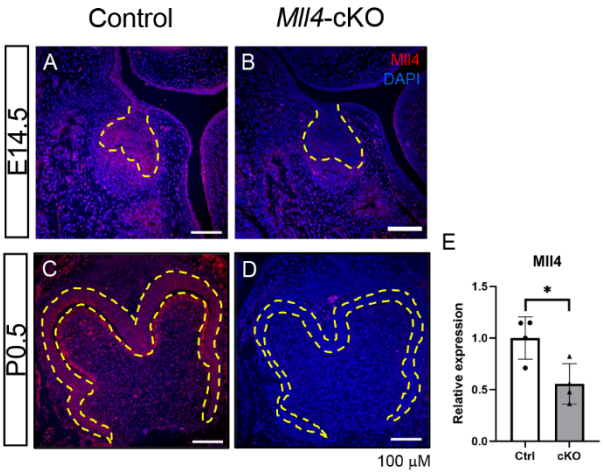

Appendix Figure 4. *Mll4*-cKO tooth germs exhibited decreased Mll4 expression in the dental epithelium. (A–D) Immunofluorescence staining for Mll4 in the first molar of control and *Mll4*-cKO mice at E14.5 (A, B) and P0.5 (C, D), showing markedly reduced Mll4 signals in the dental epithelium of *Mll4*-cKO (B, D) compared to control (A, C) tooth germs. The dental epithelium (at E14.5) and the dental epithelial ameloblast layer (at P0.5) are outlined with yellow dashed lines. (E) Real-time qPCR showing significantly decreased *Mll4* expression in the *Mll4*-cKO first molar compared to the control. *$p < 0.05$. $n = 4$ per group.

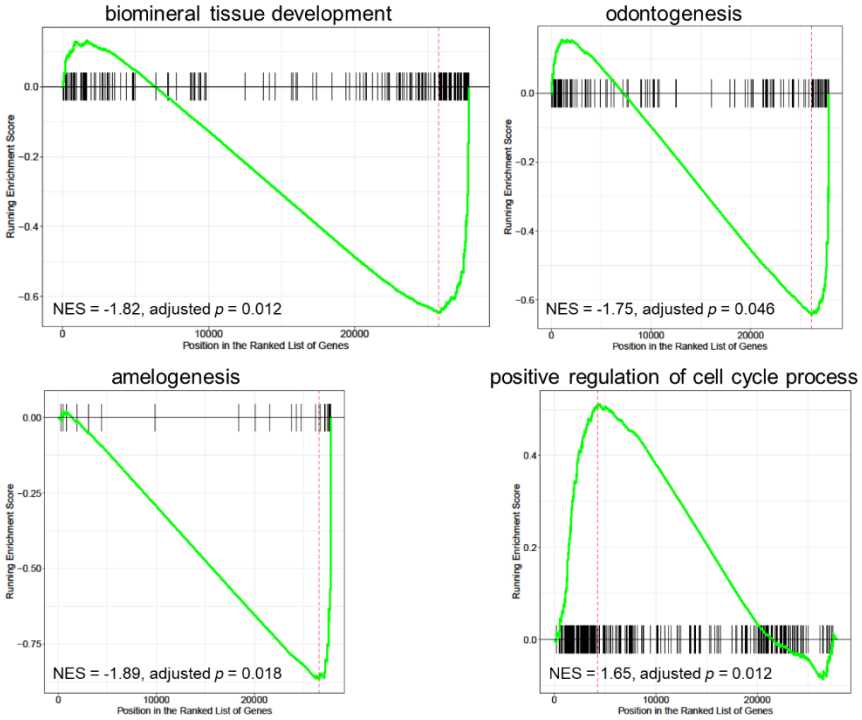

Appendix Figure 5. Gene set enrichment (GSE) analysis-based enriched biological processes in *Mll4*-cKO first molars at P0.5.

Jung-Mi Lee*, Hunmin Jung, Qinghuang Tang, Woojung An, Soo-Kyung Lee, Jae W. Lee, Yungki Park*, and Hyuk-Jae Edward Kwon*

SUPPLEMENTAL APPENDIX

Supplemental Materials and Methods

Micro-Computed Tomography (CT) Scanning and 3-Dimensional (3D) Reconstruction

The heads of 2- and 10-week-old mice were fixed overnight in 10% formalin and then rinsed with phosphate-buffered saline (PBS). Micro-CT scanning was carried out using a SCANCO µCT 100 system (SCANCO Medical, Zurich, Switzerland) with a voxel resolution of 10 µm. The obtained scans were calibrated to milligrams of hydroxyapatite per cubic centimeter (mgHA/cm^3) to ensure precise density measurements. Each image was manually adjusted for rotation and alignment along all axes using FIJI software (Schindelin et al. 2012). To reduce background noise, areas with values below 200.03 mgHA/cm^3 were excluded. Images were then cropped to isolate the specific region of interest within the first molars and incisors. Image registration was performed manually using the Fijiyama plugin for alignment (Fernandez and Moisy 2021). Finally, 3D rendering was accomplished using the 3Dscript plugin (Schmid et al. 2019).

Scanning Electron Microscopy (SEM) Imaging

Mouse mandibles were collected and fixed in 4% paraformaldehyde in 10 mM PBS at room temperature for 1 hour. After fixation, the tissues were stored overnight at 4°C. To ensure the complete removal of any residual fixative, the tissues were thoroughly washed with PBS. The gingival tissues of the mandibles were then carefully dissected to expose the teeth and surrounding periodontal structures. Importantly, decalcification was omitted to preserve the bone tissue in its natural mineralized state. The enamel was etched with 37.5% KERR Gel etchant. After etching, the specimens were rinsed with phosphoric acid and then thoroughly washed with water to remove any remaining etchant. The specimens were mounted and coated with evaporated carbon using a high vacuum evaporator (Denton 502 Evaporator, Denton Vacuum, Moorestown, NJ, USA). SEM was performed using a Hitachi SU-70 field emission SEM (Tokyo, Japan) at an accelerating voltage of 2.0 keV. Imaging was conducted using an in-lens secondary electron detector at zero tilt, or with a lower detector at a 70° tilt, to achieve detailed visualization of the molar surface structures.

Histology and Immunofluorescence Staining

Mice were euthanized at designated developmental stages. Head tissue specimens were fixed in 4% paraformaldehyde, dehydrated through a graded ethanol series, embedded in paraffin, and sectioned at a thickness of 5–7 µm, as previously reported (Lee et al. 2022). Specimens collected at E16.5 and P0.5 were decalcified in 14% ethylenediaminetetraacetic acid (EDTA) for 3 and 7 days, respectively. For histological analysis, sections were stained with hematoxylin and eosin, as previously described (Lee et al. 2022), and imaged using an Axioscope upright light microscope at 20X magnification (Zeiss, Oberkochen, Germany). An SZX16 stereomicroscope (Olympus, Tokyo, Japan) was used for capturing gross images.

For immunofluorescence staining, antigen retrieval was conducted in an antigen retrieval buffer using a pressure cooker for 15 minutes at low pressure. Sections were then washed in PBS and blocked at room temperature in a blocking buffer containing 2% goat serum, 5% BSA, 1% Triton-X 100, and 0.1% Tween-20 in PBS for 1 hour. Primary antibodies, diluted in blocking buffer, were incubated with the sections overnight at 4°C. The following day, sections were washed in PBS, incubated with secondary antibodies diluted in blocking buffer for 1 hour at room temperature, washed again in PBS, and mounted using Vectashield mounting media with DAPI (Vector Laboratories, Burlingame, CA, USA; H-1200). The primary antibody used was a homemade guinea pig anti-Mll4 (1:300) (Huisman et al. 2021). Immunofluorescence images were captured using a THUNDER Imager fluorescence microscope (Leica Microsystems, Wetzlar, Germany).

EdU Staining

EdU (5-ethynyl-2'-deoxyuridine) was administered to pregnant mice at a dosage of 10 mg/kg of body weight, one hour before the mice were euthanized. The embryos were then dissected, processed, and sectioned at a

thickness of 5 µm. EdU detection was performed using the Click-iT Plus Alexa Fluor 488 imaging kit according to the manufacturer's instructions (Invitrogen, Carlsbad, CA, USA; C10637).

TUNEL Assay

The DeadEnd™ Fluorometric TUNEL System (Promega, Madison, WI, USA; G3250) was used to assess apoptosis in paraffin sections, according to the manufacturer's protocol.

Skeletal Preparations

Mouse heads, collected at P0.5, were fixed in 100% ethanol for 3 days, stained with an Alcian Blue solution (30 mg Alcian Blue dissolved in 20 ml glacial acetic acid and 80 ml 95% ethanol) for 2 days, and then re-fixed in 100% ethanol for 24 hours. The samples were subsequently cleared in 2% KOH for 3 hours and counterstained with an Alizarin Red solution (50 mg Alizarin Red dissolved in 1 L of 1% KOH) for 24 hours. Following staining, tissue clearing was performed in 1% KOH/20% glycerol for 3 days. Images were captured using a standard stereomicroscope (Amscope, Irvine, CA, USA).

RNA-Seq and Bioinformatics Analysis

Total RNA was isolated from micro-dissected first molars of control and *Mll4* conditional knockout (cKO) mice at birth (P0.5) using the PureLink RNA Mini Kit (Invitrogen, Carlsbad, CA, USA; 12183018A). Four biological replicates per genotype, control and *Mll4*-cKO, were utilized for sequencing. Library preparation and high-throughput sequencing (Illumina, San Diego, CA, USA; NovaSeq 6000) were carried out by Novogene (Beijing, China). Sequencing reads were processed using Salmon (Patro et al. 2017) to quantify transcript-level gene expression. The resulting Salmon outputs were further analyzed using DESeq2 (Love et al. 2014) to assess gene expression at the gene level and identify differentially expressed genes (DEGs) between *Mll4*-cKO and littermate controls. DEGs were defined by a log2 fold change (log2FC) ≥ 0.4 and an adjusted p-value ≤ 0.001. Volcano plots were generated using the EnhancedVolcano package (Blighe et al. 2024). Gene ontology analysis was conducted with the clusterProfiler package (Wu et al. 2021). The RNA-seq data files have been submitted to the National Center for Biotechnology Information Gene Expression Omnibus (NCBI GEO) database under BioProject accession number PRJNA1149088.

CUT&RUN-Seq

Cells were isolated from the first molars of wild-type mice at birth (P0.5), with approximately 15,000 cells per group utilized for the CUT&RUN assay, following the manufacturer's protocol (Cell Signaling, Danvers, MA, USA; 86652). Library preparation was performed using the NEBNext UltraII DNA Library Prep Kit for Illumina (New England Biolabs, Ipswich, MA, USA; NEB#7645L) as per the provided instructions. Sequencing reads were mapped to the mouse genome (mm10) by Bowtie 2 (Langmead and Salzberg 2012). The mapping rates were 94.52% and 62.11% for the first and second replicates, respectively. The mapped reads were then analyzed by MACS3 (Zhang et al. 2008) to identify Mll4 binding peaks. For the two replicates, we identified 4,198 and 3,030 peaks, respectively. BEDTools (Quinlan and Hall 2010) identified 2,271 peaks that are common to both replicates. We used the GREAT webserver (McLean et al. 2010) for the overrepresentation analysis of gene ontology terms for the 2,271 Mll4 binding peaks. The CUT&RUN-seq data files have been deposited in the National Center for Biotechnology Information Gene Expression Omnibus (NCBI GEO) database under BioProject accession number PRJNA1149088.

Analysis of Publicly Available Single-cell RNA Sequencing (scRNA-Seq) Datasets

The scRNA-seq datasets performed on mouse P7 incisors (GSE146855) were imported into Seurat v3.6 (Stuart et al. 2019) for unsupervised clustering and cell population classification. Subsequently, dental epithelial cells were subsetted and sub-clustered to identify major dental epithelial cell types, which were then projected onto a UMAP (Uniform Manifold Approximation and Projection) plot. The expression of *Kmt2d*/*Mll4* in major dental epithelial cell types was visualized with FeaturePlot function implemented in the Seurat package. The joint expression of *Kmt2d* and its direct target genes were estimated and visualized using the Nebulosa package (Alquicira-Hernandez and Powell 2021).

Quantitative Real-Time RT-PCR (qRT-PCR)

Total RNA was extracted using the PureLink RNA Mini Kit (Invitrogen, Carlsbad, CA, USA; 12183018A) and reverse-transcribed with iScript™ Reverse Transcription Supermix (Bio-Rad, Hercules, CA, USA). Quantitative RT-PCR was conducted using the 7500 Real-Time PCR System (Applied Biosystems, Foster City, CA, USA) and SsoAdvanced Universal SYBR Green Supermix (Bio-Rad, Hercules, CA, USA). The expression levels of the target genes were normalized to *Hprt* expression. PCR reactions were performed in triplicate. Differential expression was analyzed using Student's t-test.

qRT-PCR Primer Sequences

Gene	Primer Sequence
Hprt	TGC TGG TGA AAA GGA CCT CTC G
	CTG GCA ACA TCA ACA GGA CTC C
Amelx	ATG GGG ACC TGG ATT TTG
	TTA ATC CAC TTC TTC CCG
Ambn	CAG AAG GCT CTC CAC TGC AA
	CCC CAA GGG TGT GGT AAC AT
Enam	TGC AGA AAT CCG ACT TCT CCT
	CAT CTG GAA TGG CAT GGC A

Statistics

All statistical analyses were conducted using Prism 10 software (GraphPad Software, San Diego, CA, USA). Pairwise comparisons for differential expression were assessed using Student's t-test. Statistical significance was determined with *p*-values defined as ≤ 0.05 (*), ≤ 0.01 (**), ≤ 0.001 (***), and ≤ 0.0001 (****).

References

Alquicira-Hernandez J, Powell JE. 2021. Nebulosa recovers single-cell gene expression signals by kernel density estimation. Bioinformatics. 37(16):2485-2487.

Enhancedvolcano: Publication-ready volcano plots with enhanced colouring and labeling. 2024. [accessed]. https://github.com/kevinblighe/EnhancedVolcano.

Fernandez R, Moisy C. 2021. Fijiyama: A registration tool for 3d multimodal time-lapse imaging. Bioinformatics. 37(10):1482-1484.

Huisman C, Kim YA, Jeon S, Shin B, Choi J, Lim SJ, Youn SM, Park Y, K CM, Kim S et al. 2021. The histone h3-lysine 4-methyltransferase mll4 regulates the development of growth hormone-releasing hormone-producing neurons in the mouse hypothalamus. Nat Commun. 12(1):256.

Langmead B, Salzberg SL. 2012. Fast gapped-read alignment with bowtie 2. Nat Methods. 9(4):357-359.

Lee JM, Qin C, Chai OH, Lan Y, Jiang R, Kwon HE. 2022. Msx1 drives tooth morphogenesis through controlling wnt signaling activity. J Dent Res. 101(7):832-839.

Love MI, Huber W, Anders S. 2014. Moderated estimation of fold change and dispersion for rna-seq data with deseq2. Genome Biol. 15(12):550.

McLean CY, Bristor D, Hiller M, Clarke SL, Schaar BT, Lowe CB, Wenger AM, Bejerano G. 2010. Great improves functional interpretation of cis-regulatory regions. Nat Biotechnol. 28(5):495-501.

Patro R, Duggal G, Love MI, Irizarry RA, Kingsford C. 2017. Salmon provides fast and bias-aware quantification of transcript expression. Nat Methods. 14(4):417-419.

Quinlan AR, Hall IM. 2010. Bedtools: A flexible suite of utilities for comparing genomic features. Bioinformatics. 26(6):841-842.

Schindelin J, Arganda-Carreras I, Frise E, Kaynig V, Longair M, Pietzsch T, Preibisch S, Rueden C, Saalfeld S, Schmid B et al. 2012. Fiji: An open-source platform for biological-image analysis. Nat Methods. 9(7):676-682.

Schmid B, Tripal P, Fraaß T, Kersten C, Ruder B, Grüneboom A, Huisken J, Palmisano R. 2019. 3dscript: Animating 3d/4d microscopy data using a natural-language-based syntax. Nat Methods. 16(4):278-280.

Stuart T, Butler A, Hoffman P, Hafemeister C, Papalexi E, Mauck WM, 3rd, Hao Y, Stoeckius M, Smibert P, Satija R. 2019. Comprehensive integration of single-cell data. Cell. 177(7):1888-1902.e1821.

Wu T, Hu E, Xu S, Chen M, Guo P, Dai Z, Feng T, Zhou L, Tang W, Zhan L et al. 2021. Clusterprofiler 4.0: A universal enrichment tool for interpreting omics data. Innovation (Camb). 2(3):100141.

Zhang Y, Liu T, Meyer CA, Eeckhoute J, Johnson DS, Bernstein BE, Nusbaum C, Myers RM, Brown M, Li W et al. 2008. Model-based analysis of chip-seq (macs). Genome Biol. 9(9):R137.

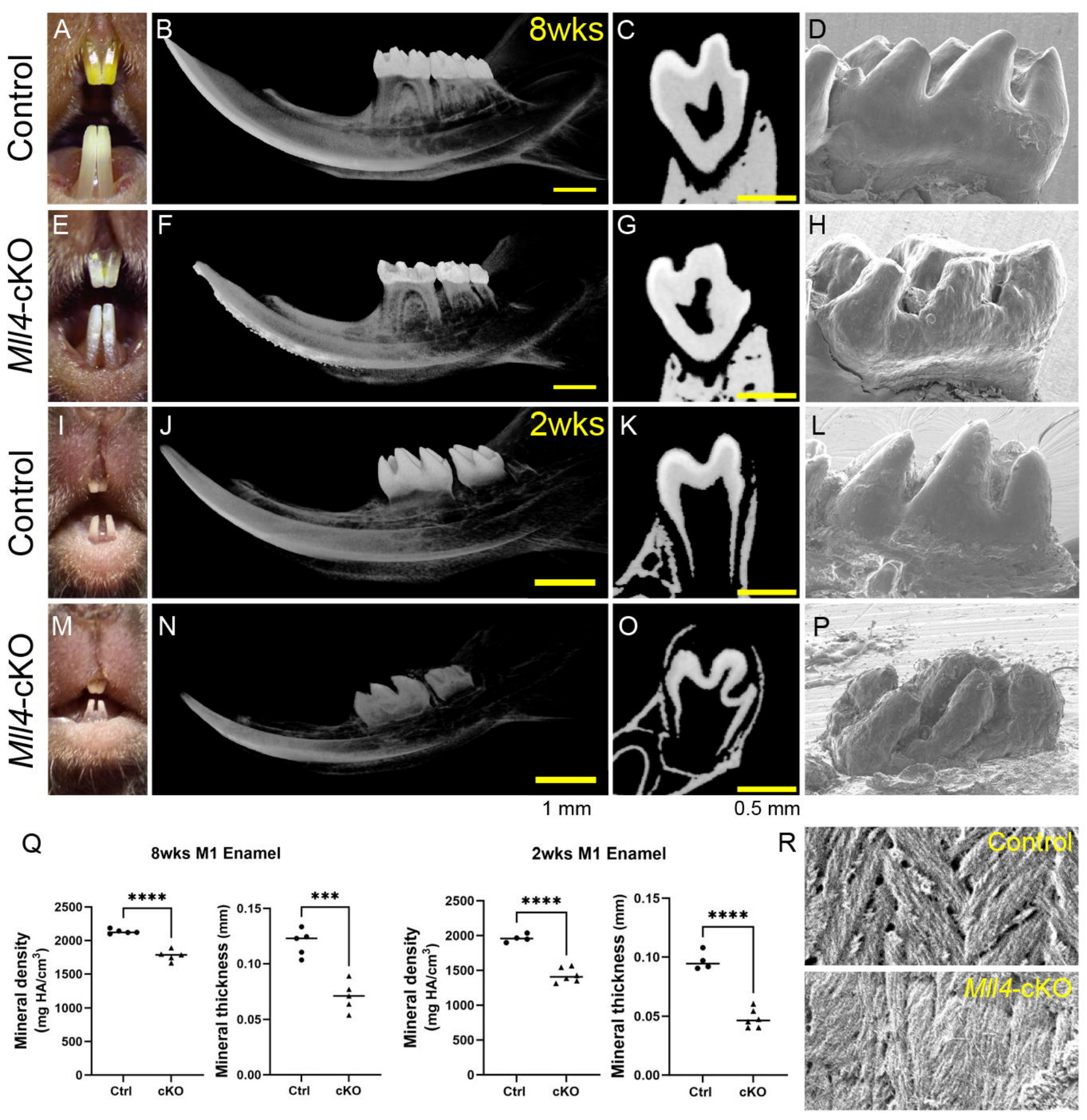
Control
Mll4-cKO
Control
Mll4-cKO
A
B
8wks
C
D
E
F
G
H
I
J
2wks
K
L
M
N
O
P
1 mm
0.5 mm
Q
8wks M1 Enamel
2wks M1 Enamel
Mineral density (mg HA/cm3)
Mineral thickness (mm)
Ctrl
cKO
****
***
R
Control
Mll4-cKO

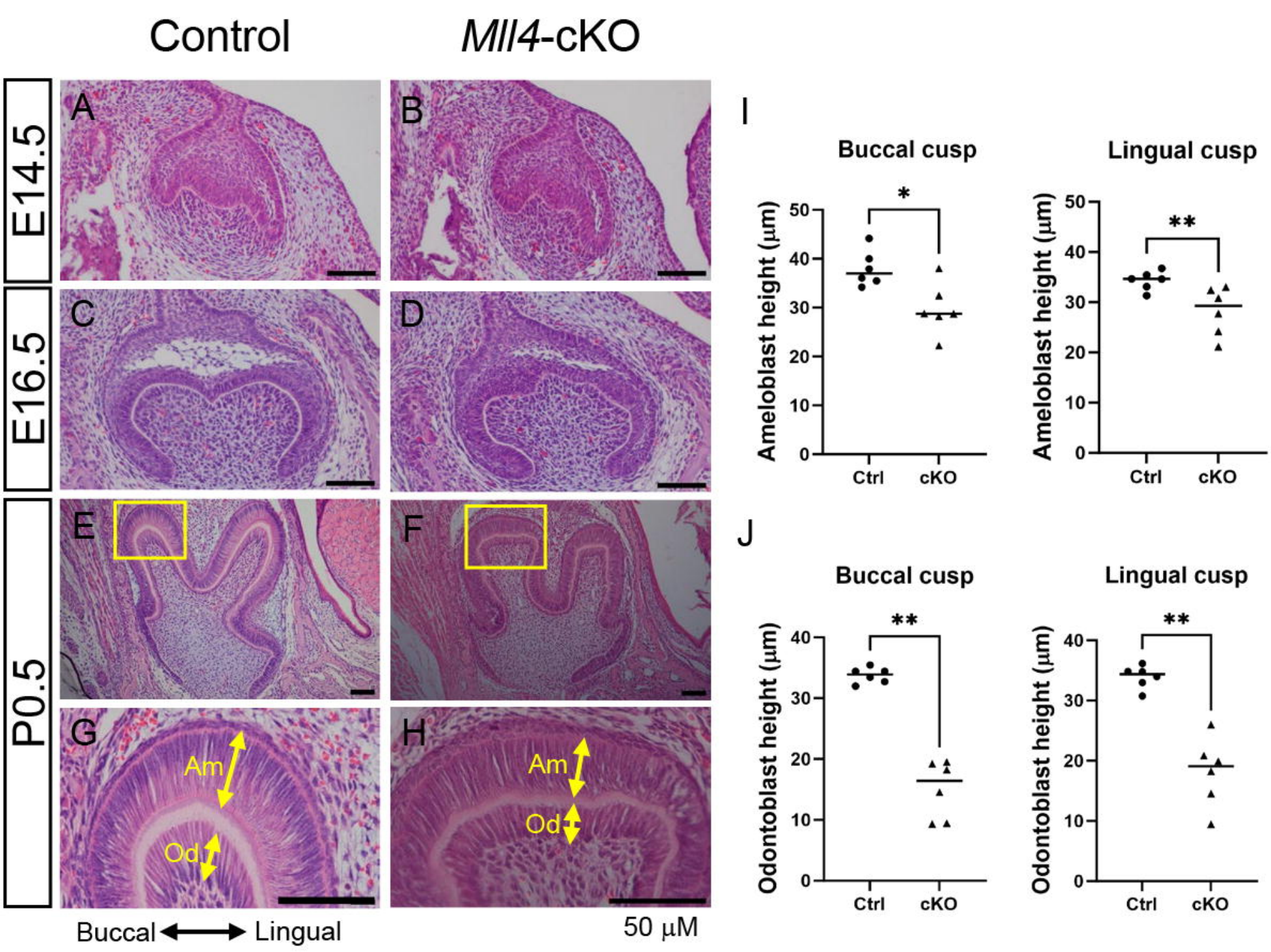
Control
Mll4-cKO
E14.5
E16.5
P0.5
A
B
C
D
E
F
G
H
Am
Od
Buccal
Lingual
50 μM
I
Buccal cusp
Lingual cusp
Ameloblast height (μm)
0
10
20
30
40
50
*
**
Ctrl
cKO
J
Buccal cusp
Lingual cusp
Odontoblast height (μm)
0
10
20
30
40
**
Ctrl
cKO

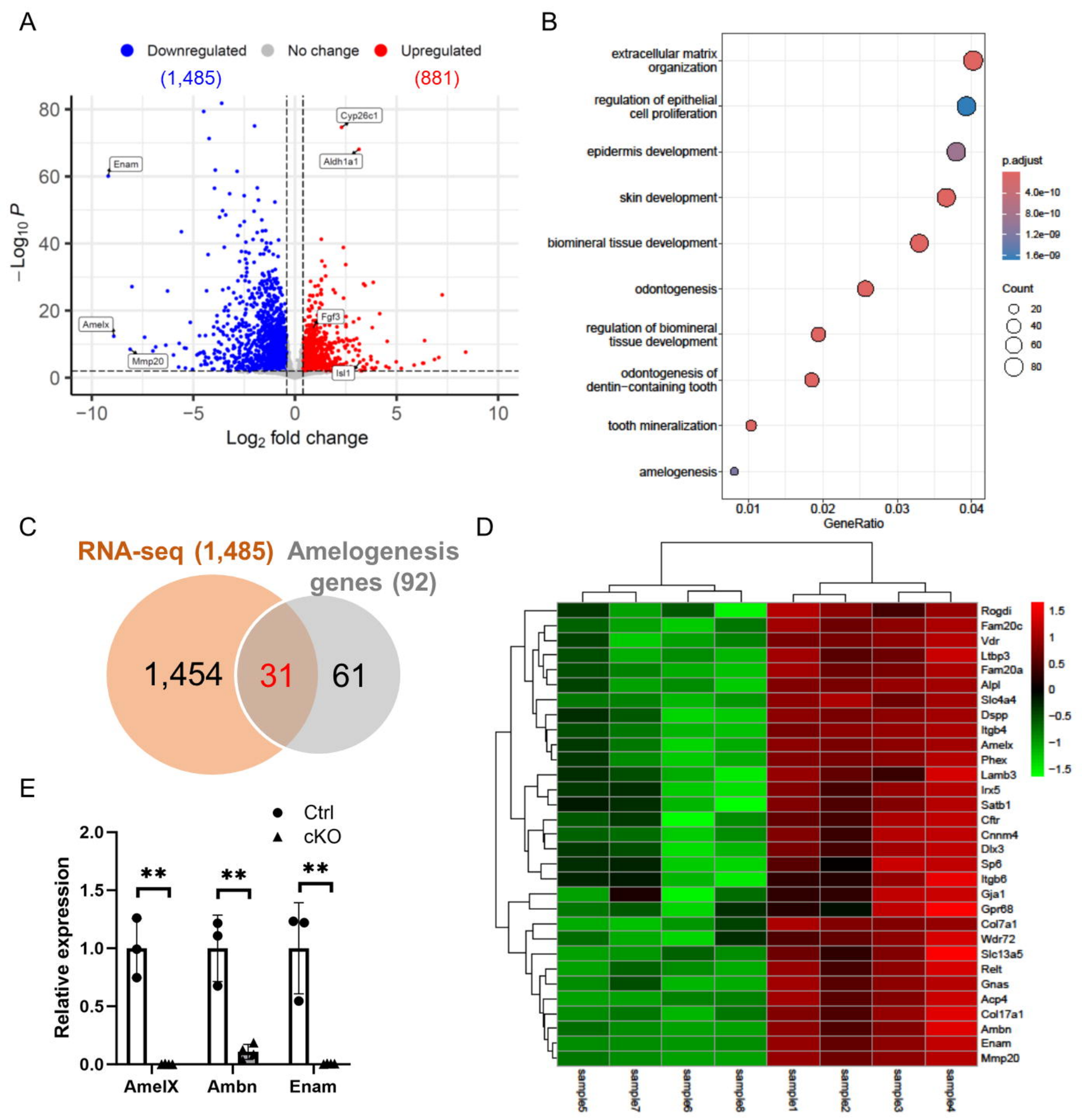
A
Downregulated
No change
Upregulated
(1,485)
(881)
Cyp26c1
Aldh1a1
Enam
Fgf3
Amelx
Mmp20
Isl1
−Log10 P
Log2 fold change
B
extracellular matrix organization
regulation of epithelial cell proliferation
epidermis development
skin development
biomineral tissue development
odontogenesis
regulation of biomineral tissue development
odontogenesis of dentin−containing tooth
tooth mineralization
amelogenesis
GeneRatio
p.adjust
Count
C
RNA-seq (1,485)
Amelogenesis genes (92)
1,454
31
61
D
Rogdi
Fam20c
Vdr
Ltbp3
Fam20a
Alpl
Slc4a4
Dspp
Itgb4
Amelx
Phex
Lamb3
Irx5
Satb1
Cftr
Cnnm4
Dlx3
Sp6
Itgb6
Gja1
Gpr68
Col7a1
Wdr72
Slc13a5
Relt
Gnas
Acp4
Col17a1
Ambn
Enam
Mmp20
sample5
sample7
sample6
sample8
sample1
sample2
sample3
sample4
E
Ctrl
cKO
Relative expression
AmelX
Ambn
Enam

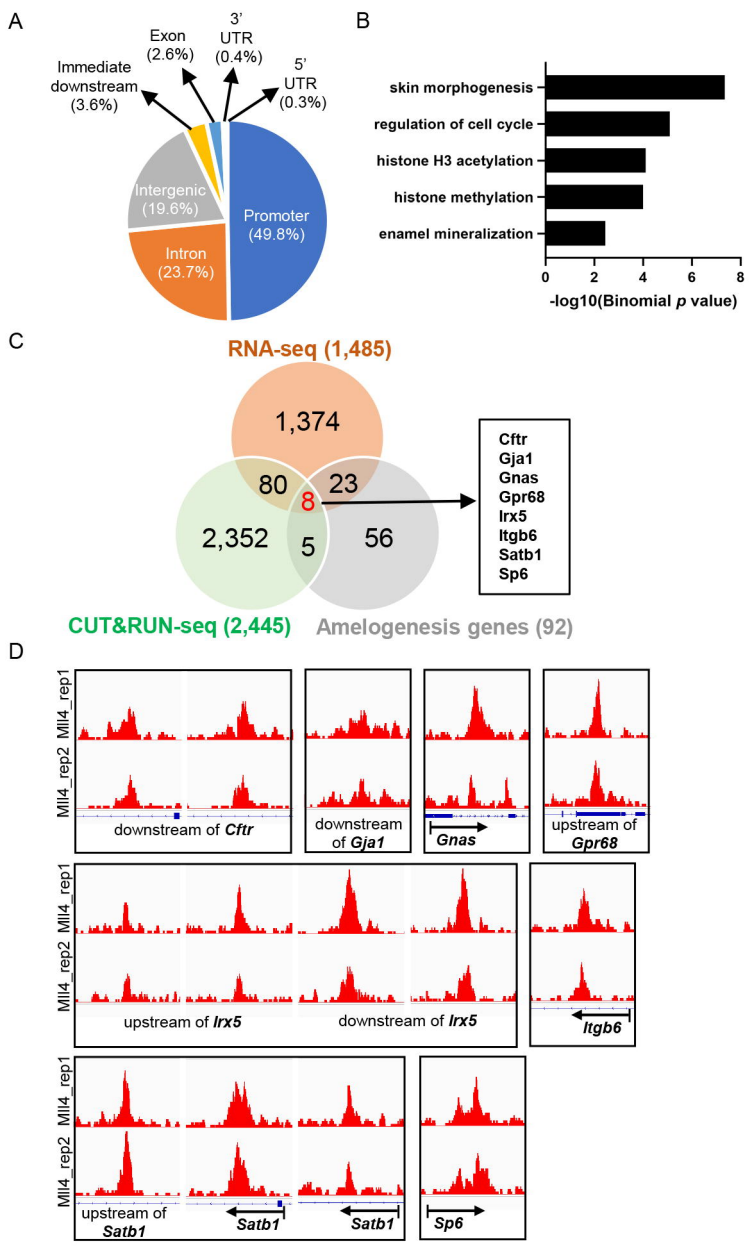
A
Exon (2.6%)
3' UTR (0.4%)
5' UTR (0.3%)
Immediate downstream (3.6%)
Intergenic (19.6%)
Promoter (49.8%)
Intron (23.7%)
B
skin morphogenesis
regulation of cell cycle
histone H3 acetylation
histone methylation
enamel mineralization
0
2
4
6
8
-log10(Binomial p value)
C
RNA-seq (1,485)
1,374
80
23
8
2,352
5
56
Cftr
Gja1
Gnas
Gpr68
Irx5
Itgb6
Satb1
Sp6
CUT&RUN-seq (2,445)
Amelogenesis genes (92)
D
Mll4_rep1
Mll4_rep2
downstream of Cftr
downstream of Gja1
Gnas
upstream of Gpr68
upstream of Irx5
downstream of Irx5
Itgb6
upstream of Satb1
Satb1
Satb1
Sp6

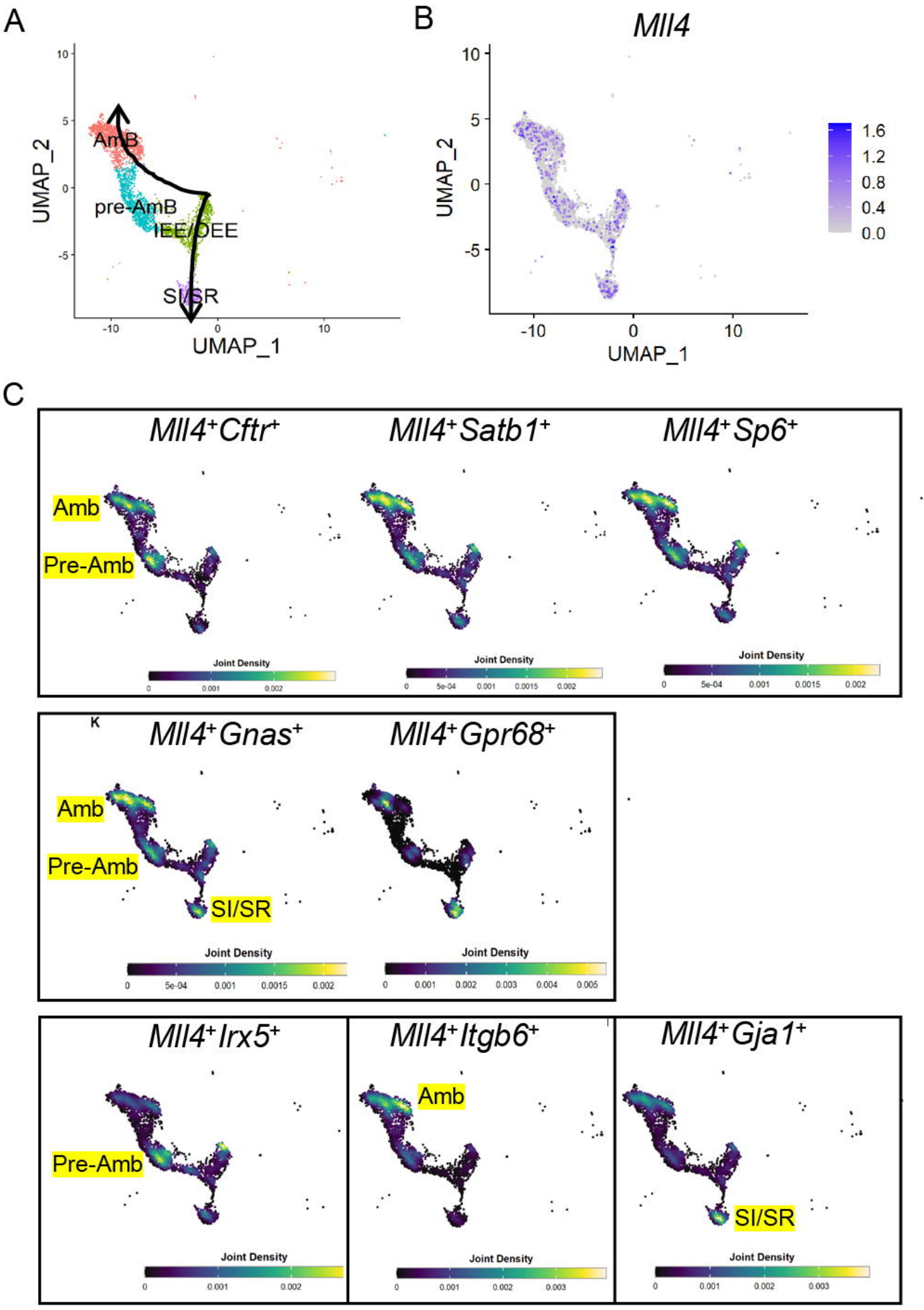
A
AmB
pre-AmB
IEE/OEE
SI/SR
UMAP_1
UMAP_2
B
Mll4
1.6
1.2
0.8
0.4
0.0
C
Mll4+Cftr+
Mll4+Satb1+
Mll4+Sp6+
Amb
Pre-Amb
Joint Density
K
Mll4+Gnas+
Mll4+Gpr68+
SI/SR
Mll4+Irx5+
Mll4+Itgb6+
Mll4+Gja1+